Linear-to-quadratic transition in electronically stimulated sputtering of solid N_2 and O_2

R. E. Johnson and M. Pospieszalska
Department of Nuclear Engineering and Engineering Physics, University of Virginia, Charlottesville, Virginia 22901

W. L. Brown
AT&T Bell Laboratories, Murray Hill, New Jersey 07974

(Received 12 November 1990; revised manuscript received 6 March 1991)

Electronic excitations produced by MeV protons and helium ions lead to ejection of molecules from solid N_2 and O_2. The yield is shown to be determined by the near-surface excitation density, rather than the primary ionization cross section. It is linear in the excitation density at low excitation densities and quadratic at high excitation densities. The linear yield can be described by discrete, nonradiative transfers of electronic energy into kinetic energy ("spikes") that utilize $\lesssim 12\%$ of the total electronic energy deposited for N_2 and $\lesssim 37\%$ for O_2. A statistical model is used to calculate the transition from low to high excitation density due to the overlap of either Maxwellian or non-Maxwellian spikes. It is found that the separate N_2 and O_2 data sets are consistent in this model, that excitations do not diffuse very far from where they are created, that the linear-to-quadratic transition is described better by the non-Maxwellian spikes, and that the energy derived in the linear regime is adequate to account for the nonlinear yields.

I. INTRODUCTION

Following the deposition of electronic energy in low-temperature condensed-gas solids, energetic nonradiative relaxation processes can lead to molecular ejection (sputtering).[1] Therefore, the analysis of sputtering data can help determine the nonradiative pathways occurring in these electronically insulating materials. Extracting this information has been complicated by the faster-than-linear character of the sputtering yields for many condensed-gas solids.[2] Recently, Johnson *et al.*,[3] defined three separate regimes of electronically induced sputtering by fast ions. For normal incidence the yields exhibit linear, quadratic, and cubic dependencies on the density of excitation along the incident ion's path. Here the transition from a linear to a quadratic sputtering yield is examined based on data for solid N_2 (Ref. 4) and O_2 (Ref. 5).

Yields that are linear in electronic excitation density can be expected when individual excitation events release sufficient energy to overcome the material cohesive forces, and they occur with sufficient separation in space or time so as not to contribute collectively.[1,3] This separation is determined by the initial distribution of excitations and by those solid-state processes that disperse the excitations and control the relaxation rates.[6] Linear yields have been reported for a number of low-temperature condensed-gas solids by keV electrons and MeV protons.[4-9] Since a large fraction of the electronic energy is deposited by fast ions as electron-hole pairs, these linear yields have been interpreted as primarily due to energy-transfer events, which are analogous to dissociative recombination in gas-phase reactions. That is, we assume neighboring atoms repel each other following the recombination of secondary electrons with localized holes.[1-11] Such events are also used to describe electronically stimulated desorption of adsorbed gases,[12] defect production in alkali halides,[13] and the dissociation of excited clusters.[14]

Sputtering yields, which vary faster than linear with the excitation density, are sensitive to the dispersal of the deposited energy. Therefore, understanding the transition from linear to quadratic can help to quantify this process. Such transitions have been observed in collisional sputtering of both metals[15] and condensed-gas solids,[7,8,10,16,17] being produced by the overlap of the kinetic energy spikes.[18-21] In electronic sputtering this overlap also occurs producing[3] a quadratic regime in which ejection depends only on the local energy density at the surface, a sublimationlike process, and a cubic regime in which it depends on the pressure gradient established. The incident angle dependence of the yield for low-temperature CO and O_2 sputtered by MeV He^+ was shown to be well predicted by the sublimationlike process.[5,22] Therefore, in this paper the instantaneous surface energy density is used to calculate the N_2 and O_2 yields.

Because the electronic-relaxation pathways can be affected by increasing excitation density, viz., the decrease in the luminescence efficiency,[23] it is important to establish whether the variation in the electronic sputtering yield can be explained by the overlap of the individual energy-transfer events. We first review the data sets for the sputtering of N_2 and O_2 by protons and helium ions as published elsewhere, and in Sec. III we give a formulation for calculating the yield based on a distribution of spikes. In Sec. IV, we use data in the linear regime to determine the fraction of the electronic energy that participates in sputtering, and then use this in Sec. V to calculate the linear-to-quadratic transition. In Sec. VI we give the standard spike calculation for comparison with the appendix containing many of the expressions used.

II. MEASURED YIELDS

The measured yields[1,4,5] were obtained elsewhere by bombardment of solid N_2 and O_2 with MeV hydrogen and helium ions.[4,5] The films, grown in a UHV chamber by condensation on a ~10-K metal surface, were approximately 4×10^{17} molecules/cm^2 thick. The predominantly neutral relative yields, independent of thickness and beam current,[9,24,25] were determined using a quadrupole mass spectrometer (QMS). To minimize the background, the nitrogen films were grown of $^{15}N_2$. Absolute sputtering yields were determined for 1.5-MeV He^+ and He^+ ions on N_2 and 2.0-MeV He^+ on O_2 using Rutherford backscattering, and the QMS yields were normalized to these values (Tables I and II). To measure the sensitivity of the sputtering yield to the incident charge state (Table I), a 20-μg/cm^2 carbon foil covered the final aperture to produce charge-state equilibrated helium ions.[4,5]

The sputtering yield data (Table I) for protons and charge-state equilibrated He^+ ions are shown in Fig. 1(a) for solid $^{15}N_2$ as a function of the equilibrium electronic stopping power,[26] S_e, and as a function of the gas-phase ionization cross section,[27] σ_I, in Fig. 1(b). It is seen that for the equilibrated helium ions there is a striking consistency with the proton yields. Using the primary ionization cross sections does not change this consistency. However, in Fig. 1(b) it is seen that the He^+ and equilibrated He^+ yields have *different* values at the same value of the primary ionization cross section. This indicates the primary ionization cross-section quantity is *not sufficient* to characterize the yield. If that is the case, then ionizations by the secondary electrons must also contribute to sputtering, so that some fraction of S_e, which describes the total energy loss of an ion, is appropriate for the ion velocities considered here. (Earlier we showed[1] that at significantly *lower* velocities, the scaling with S_e changes.)

Because sputtering is a surface phenomena, we give in Table III calculated values of α_e, which is the fraction of S_e deposited in a volume close to the surface and depends on ion speed and volume size. These are less than unity for incident ions because the secondary electrons are forward directed.[28] For a very fast ion α_e is about 0.4, which corresponds to only primary ionization in the near surface volume. In Fig. 1(b) we use values of α_e from Table III to plot the N_2 yield for incident protons versus $\alpha_e S_e$. Although the dependence of the yield is somewhat less steep, because of the increasing α_e for slower ions, it is roughly similar to that for S_e. The size of the α_e may be reduced by excitation transport, but the difference in the He^+ and equilibrated He^+ yields indicates that such transport *does not* occur over distances of the order of the average secondary electron transport distance, ~5 nm (Ref. 28). Because the dependence of α_e on ion velocity is uncertain, we use a fixed α_e for examining the linear-to-quadratic transition, realizing its limitations.

III. GENERAL DESCRIPTION OF YIELDS

The individual electronic excitation events, produced by an incident ion along its path through the solid, can lead to an impulsive transfer of energy into local kinetic energy by a variety of processes.[29] For condensed, low-

TABLE I. Sputtering yields solid for $^{15}N_2$ at 10 K.

Ion	Energy (MeV/amu)	Y	S_e (10^{-15} eV cm^2/molecule)[a]	σ_I (10^{-16} cm^2)[b]
H^+	2.5	0.5	5.5	0.73
	1.5	0.7	7.8	1.1
	1.0	0.9	10.0	1.5
	0.8	1.1	12.5	1.8
	0.5	1.6	16.5	2.4
	0.36	2.1	20.5	3.0
	0.32	2.4	22.0	3.2
	0.26	2.65	24.0	3.6
	0.20	3.4	28.2	4.2
He^+	1.0	4.1		2.8 (3.8)
	0.75	5.3		3.4 (4.4)
	0.67	7.0		3.8 (4.8)
	0.50	9.8, 9.5		4.3 (5.7)
	0.375	13.5,14.0,14.5[c]		5.7 (6.7)
$(He^+)_{eq}$	1.0	6.8	42.5	6.0 (1.95)[d]
	0.75	8.4	50.0	7.2 (1.95)
	0.67	11.5	55.0	8.0 (1.9)
	0.50	14,17.0	63.0	9.5 (1.9)
	0.375	22, 24.5[c]	78.0	11.4 (1.8)

[a]Equilibrium stopping cross section in bulk N_2 (Ref. 26).

[b]Ionization cross sections from Ref. 27. For He^+ used σ_+, positive ions produced, as charge transfer contribution is small. In brackets is given σ_-, total electron production indicating the significant $He^+ \rightarrow He^{++} + e$ contribution. The difference between these is σ_{12}. Data at energies greater than 2 MeV are extrapolations.

[c]Repeated absolute measurements. Rook, Johnson, and Brown (Ref. 24) obtained a yield of 17 for (0.375 MeV/amu) He^+ and 9.5 for (0.15 MeV/amu) He^+.

[d]For σ_I for $(He^+)_{eq}$ we use proton value of σ_I times the square of Z, which is given in brackets.

TABLE II. Sputtering yields for solid O_2 at 10 K (Ref. 5).

Ion	Energy (MeV/amu)	Y[a]	S_e (10^{-15} eV cm^2/molecule)
H^+	3.5	0.96	4.8
	3.0	1.1	5.4
	2.5	1.24	6.0
	2.0	1.15	7.0
	1.5	1.7	9.0
	1.0	2.7	11.0
	0.8	4.7	13.2
	0.5	4.8	17.6
	0.35	5.5	22.0
	0.3	7.3	23.8
$He^+(He^{q+})$[b]	0.75	27 (32)	54.0
	0.635	41 (49)	60.0
	0.5	60 (72)	70.0
	0.375	75 (90)	84.0
	0.25	140 (170)	94.0

[a]Quadrupole data of Ref. 5, normalized to Rutherford backscattering spectroscopy (RBS) yield for 2.0 MeV He^+, $Y \approx 60$. (Note it was incorrectly stated in Ref. 5 that the yields were normalized to $Y \approx 54 \pm 5$ the RBS yield from Ref. 24. The latter yields disagree somewhat with the more recent measurements of the yields in Ref. 5.)

[b]Note that the values of S_e are equilibrium stopping cross sections and apply to equilibrated He^+. The ratio of the yield of He^+ to equilibrated He^+ is about 1.2 ± 0.1 in this region. We use 1.2 for the values in brackets which are used in Fig. 2.

temperature N_2 and O_2, dissociation events beneath the surface are assumed to drive the sputtering and to occur rapidly. Therefore, the spatial distribution of these events determines the calculation of the average yields, $\bar{Y}$,

$$\bar{Y} = \sum_I w_I Y_I[\mathbf{r}_1, \mathbf{r}_2, \ldots] \ . \tag{1a}$$

Here Y_I is the yield for a distribution of events located at $\mathbf{r}_1, \mathbf{r}_2, \ldots$ labeled I, produced by a single incident ion and w_I is the weight factor for this distribution. For a fast ion, which does not slow down significantly over the region of interest, the events are distributed randomly in depth and radially from the track. The spatial distribution of interest is that occurring at the time of repulsive decay,[1] which can differ from the initial distribution due to excitation diffusion, enhancing trapping, and decay at the surface.[30] Ignoring this and the small radial distribution, the Poission probabilities can describe w_I, so that Eq. (1) becomes

$$\bar{Y} = \int dz_1 \int dz_2 \int dz_3 \cdots P_1(z_1) P_2(z_2) \cdots Y_I[z_1, z_2, \ldots] \ . \tag{1b}$$

Here $P_i(z_i)dz_i$ is the probability that the ith event occurs between depth z_i and $z_i + dz_i$, where

$$P_i(z_i) = \exp[-(z_i - z_{i-1})/\lambda_e]/\lambda_e \ ,$$

for $z_i \geq z_{i-1}$ and $P_i(z_i) = 0$, $z_i < z_{i-1}$, with $z_0 = 0$, and λ_e is the mean spacing between events. For perpendicular incidence Y_I in Eqs. (1a) or (1b) can be written quite generally as[22,29,31]

$$Y_I = \int d^2\rho \int dt \ \Phi(I; \boldsymbol{\rho}, t) \ , \tag{2}$$

where Φ is the time-dependent flux of neutrals leaving a region of the surface labeled by the radial distance about the particle track, ρ. These forms will be used to calculate the yield as a function of the mean spacing between events, λ_e. Limiting cases are considered first.

In the limit that λ_e is very small, the Y_I are all roughly the same, therefore, Eqs. (1a) and (1b) become well approximated by

$$\bar{Y} = \int d^2\rho \int dt \int \Phi(\lambda_e; \rho, t) \equiv Y_c \ , \tag{3}$$

so that yield depends directly on the average spacing of events giving the cylindrical spike yield, Y_c. This yield is quadratic in λ_e^{-1} (see the Appendix) if Φ depends on ρ and t *only* through the value of the surface energy density,[22] an assumption found for these solids to give the

TABLE III. Fraction of electronic energy loss deposited as excitations and ionizations in the near surface layer. Estimated using data in Ref. 35 for protons in H_2O. Fractions of $n_m S_e$ deposited in first 1 nm from the surface or first 3 nm from the surface.

E/M (MeV/amu)	α_e(1 nm)	α_e(3 nm)
3.0	0.43±0.05	0.55±0.05
2.0	0.43	0.55
1.5	0.43	0.57
1.0	0.45	0.60
0.75	0.50	0.65
0.50	0.58	0.73
0.25	0.68	0.85

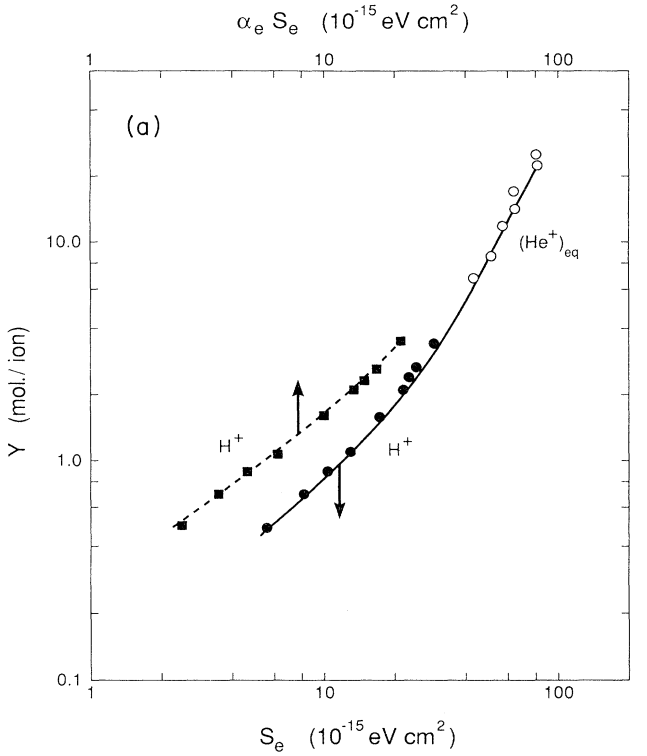

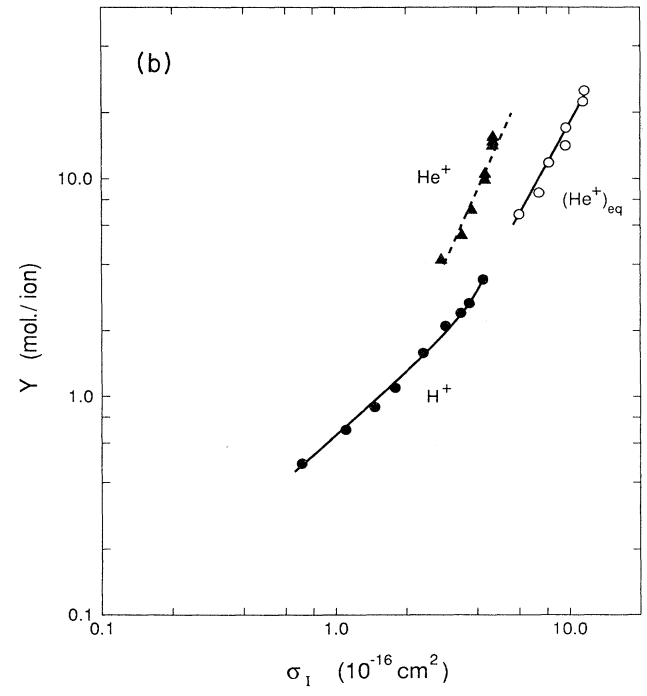

FIG. 1. (a) Measured yields of N_2 molecules removed per ion incident for H^+ and $(He^+)_{eq}$ vs equilibrium stopping cross section. Yield data are plotted using $\alpha_e S_e$ for protons for 1 nm volume in Table III using appropriate velocity. (b) Measured yields of N_2 vs primary ionization cross section, σ_I, Ref. 27 (viz., Table I), for H^+, He^+, and $(He^+)_{eq}$.

correct dependence of the yield on incident angle at small λ_e.[5,22] (If Φ depends on ρ and t via the net volume force, a different dependence is observed as discussed elsewhere.[3])

At "low" excitation densities the events are widely spaced in depth and/or time producing sputtering independently so that $Y_I = \Sigma Y(z_i)$, where $Y(z_i)$ is the yield from an individual event at depth z_i. Using this, Eq. (1b) reduces to a single integral,

$$\bar{Y} = \int dz \left[\sum_{i=1}^{\infty} (z^{i-1}/\lambda_e^i) \exp(-z/\lambda_e) \right] Y(z)$$
$$= \lambda_e^{-1} \int Y(z) dz \ . \tag{4a}$$

This gives a yield linear in λ_e^{-1}, which can be written

$$\bar{Y} = Y_l \equiv (\Delta\bar{z}/\lambda_e) \ , \tag{4b}$$

where $\Delta\bar{z}$ is the weighted sputter depth as in Eq. (3a) of Ref. 1. Here we are interested in the transition from this linear yield to the cylindrical, quadratic yield of Eq. (3) as λ_e decreases. First, we note from Eq. (4a) that the linear yield, Y_l, already includes contributions to sputtering from other than the excitation closest to the surface. The contribution to $\bar{Y}$ due to the first excitation *alone* can be written as

$$Y_1 = \int dz_1 P_1(z_1) Y(z_1) \approx \Delta\bar{z}/(\lambda_e + \Delta s) \ , \tag{5}$$

where we assumed, for convenience, $Y(z) \approx Y_0 e^{-z/\Delta s}$, where Y_0 is the yield in the surface monolayer and Δs is a mean depth from which the deposited energy contributes to sputter ejection (i.e., $\Delta\bar{z} = Y_0 \Delta s$). Equation (5) is seen to be linear *only* for $\lambda_e \gg \Delta s$. In the following we first estimate the energy of the individual events in the linear regime using Eq. (4b) and then use Eqs. (1a) or (1b) to describe the transition in the yield as λ_e decreases.

IV. LINEAR YIELDS

For sputtering due to individual events, molecular dynamics calculations for amorphous condensed-gas solids[33,34] indicate that a collision cascade expression can be used to describe the dependence of the yield on the average energy per event, $\overline{\Delta E}$. That is, the sputter depth in Eq. (4b) simplifies to[1]

$$\Delta\bar{z} \approx (c/n_m \bar{\sigma}_d)(\overline{\Delta E} - U)/U \ , \tag{6}$$

where $\bar{\sigma}_d$ is the effective interaction (diffusion) cross section and c is a proportionality constant (see the Appendix). U and n_m are the material cohesive energy and molecular number density (Table IV). Based on the molecular dynamics calculations, $c/n_m\bar{\sigma}_d \approx 0.14l$ (see the Appendix) with $l \approx n_m^{-1/3}$ (roughly a layer thickness). Using α_e and writing $(dE/dx)_e$ as $n_m S_e$, the mean spacing between excitations in the near surface layers is obtained: $\lambda_e^{-1} \approx \alpha_e n_m S_e / W_s$, where W_s is the average electronic energy deposited per excitation leading to an average energy releases $\overline{\Delta E}$. Using Eqs. (4b) and (6) the yield can also be written[10,11,24]

TABLE IV. Molecular properties.

Molecule	n_m (10^{22} molecule/cm^3)	l (nm)	I (eV)	U (eV)	W (eV)
N_2	2.2	0.36	15.6	0.075	36.2 (He^+) 37.0 (H^+)
O_2	2.4	0.35	12.2	0.095	32.5

$$Y_l \approx c\alpha_e (f_s S_e)/\bar{\sigma}_d U \ , \tag{7}$$

where $f_s = \overline{\Delta E}/W_s$ and $\overline{\Delta E} \gg U$. Such a form, also obtainable by dimensional arguments, resembles the collision cascade expression,[31,32] with $(f_s S_e)$ replacing the elastic nuclear stopping cross section. The yields for high-energy protons are consistent with $(\alpha_e f_s) \approx 0.05$ for N_2 and $(\alpha_e f_s) \approx (0.16)$ for O_2. Extracting f_s or α_e separately requires additional assumptions.

Assuming $\alpha_e = 0.43$ (see Table III) for the proton data in Table I implies a yield for 2-keV electrons on N_2 [$\alpha_e \approx 1.2$ (Ref. 9)] of about 0.8 molecules/electron, somewhat smaller than the measured yield of Ellegard and coworkers,[7,9] of 1.2. If the distances for excitation transport[30] are large, the α_e's for electrons and protons would be closer in value, increasing the discrepancy. This comparison reinforces the conclusion that diffusive transport distances in electronic sputtering of N_2 and O_2 are smaller than the secondary electron transport distances. Therefore, using an $\alpha_e \gtrsim 0.43$ for the proton data, $f_s \lesssim 0.12$ for N_2 and $f_s \leq 0.37$ for O_2. To estimate $\overline{\Delta E}$ from f_s, since W_s in the solid is likely to be less than the gas phase W value for ionization[35,36] (Table IV), then $\overline{\Delta E}$ is less than or equal to 4.4 eV and 12 eV for N_2 and O_2, respectively, consistent with other estimates.[24,25] Because it is unlikely for outer shell processes that 12 eV would be deposited in a single decay, a sequence of nonradiative relaxation processes spaced closely in time may be involved.[24,25]

The above implies that sputtering in the linear regime is due to either the first event [$\lambda_e \gg \Delta s$ in Eq. (5)] *or* contributions also come from second, third, etc., events, which are displaced radially or in time, a consideration in elastic nuclear sputtering also.[37] Using $\Delta s \approx 3l$[33,34] in Eq. (5), even for a 1-MeV proton, for which $\lambda_e \approx 10l$, with $\alpha_e \approx 0.5$ and $W_s \approx 37$ eV for N_2, it is seen that Y_1 is about 70% of the calculated $\bar{Y}$. This indicates that "second" excitations contribute to the "linear" yield at this λ_e. Below, we consider the distribution of events more carefully.

V. NONLINEAR YIELDS

The transition in the yield from linear to quadratic with increasing $(dE/dx)_e$ can arise from overlapping events ("spikes") fueled by the ΔE[1,10] determined above. Here we test this concept using Eq. (1a) assuming the same energy per event for all λ_e with the statistically distributed spikes contributing cooperatively by increasing the transient surface kinetic energy density[3] above that produced by an individual spike. As the density of events along the track of a single incident ion λ_e^{-1} increases, the spikes merge, eventually producing a uniformly energized cylindrical region, Eq. (3).

In order to calculate Y_I for use in Eq. (1a) two different expressions for the dependence of the "flux" of escaping molecules, [Φ in Eq. (2)], are used. One expression is based on a local equilibrium (Maxwellian) energy distribution for each spike and the other assumes equilibration does not occur during sputtering, with each molecule having the local average energy, a δ-function distribution (see the Appendix). For the kinetic-energy transport in the material a constant diffusivity is assumed so that the total kinetic-energy density distribution for a group of spikes along an ion track can be obtained by addition.[3,5,22,38] For a diffusivity that is not constant (see the Appendix), the evolution of the energy must be obtained by solving the diffusion equation for each particular spatial distribution of spikes. Typically the diffusivity depends only weakly on the local energy density.[39] For constant diffusivity the local average energy per molecule for a single spike is

$$\bar{E}(r_i,t) = \frac{\overline{\Delta E}}{\pi^{3/2} n_m} \frac{\exp[-r_i^2/\Delta(t)^2]}{\Delta(t)^3} \ , \tag{8}$$

where $\Delta(t) = [4\kappa(t+t_0)]^{1/2}$ is the radial size of a spike, which increases with time (see the Appendix), κ is the "thermal" diffusivity, and t_0 gives an initial width.[40] Assuming that the nonradiative, electronic relaxation times are fast compared to the kinetic-energy transport times ($\sim 10^{-12}$–10^{-11} s), all the events in Eq. (1a) have the same start time, $t=0$. Now the $Y_I[\mathbf{r}_1, \mathbf{r}_2, \ldots]$ are calculated from Eq. (2) using a particular surface ejection function with spikes located at $\mathbf{r}_1, \mathbf{r}_2, \ldots$ as in Eq. (A7). These spikes are *randomly* distributed in depth, with a mean spacing of λ_e, and radially within a cylinder $\bar{r}$. To calculate an average yield we set w_I in Eq. (1a) equal to one for each distribution chosen using a Monte Carlo selection of depths. When $\bar{r}=0$, events in a line, then we compare to calculations using Eq. (1b). A sufficient depth is used in each calculation so the yield is independent of sample size. The Y_I are calculated using the total-energy density at the surface[3,38–40] for a number of spatial distributions corresponding to the same λ_e and are then averaged to obtain $\bar{Y}$. λ_e and Δ_0 are the input parameters for each set of calculations, where Δ_0 is an intrinsic spike radius from Eq. (8) [i.e., $\Delta_0^3 \equiv \overline{\Delta E}/(n_m U \pi^{3/2})$]. We used the upper limits, $\overline{\Delta E} \approx 4.4$ eV for N_2 and $\overline{\Delta E} \approx 12$ eV for O_2 giving $\Delta_0 \approx 2.1l$ and $2.9l$, respectively, of the order of Δs used earlier.

The ratios of the calculated average yield to the linear yield Y_l, $\bar{Y}/Y_l$ versus Δ_0/λ_e, were found to depend only

very weakly on the $\overline{\Delta E}$ chosen (i.e., Δ_0) over a reasonable range of $\overline{\Delta E}$, reducing the importance of determining $\overline{\Delta E}$ accurately when considering the transition from linear-to-quadratic yields. Plotting this ratio also eliminates consideration of the efficiency of ejection in the calculation and the importance of the normalization of the data sets. Therefore, it is seen in Fig. 2 that the data sets for N_2 and O_2 plotted as $\bar{Y}/Y_l$ versus Δ_0/λ_e are remarkably consistent with each other, allowing for the larger scatter in the O_2 data. This indicates that Δ_0/λ_e is a useful parameter in the transition region, where we used $\alpha_e=0.65$, a value intermediate to those in Table III. Varying α_e would stretch the curve in Fig. 2.

The curve drawn through the data in Fig. 2 is compared to the calculated ratios in Fig. 3 labeled by $(\Delta(0),\bar{r})$ for a set of spikes with a chosen initial ($t=0$) radius $\Delta(0)$ and distributed uniformly in a radius $\bar{r}$ about an ion track. Calculations are shown for an escape flux based on Maxwellian [Fig. 3(a)], representing a broad distribution, and a δ function [Fig. 3(b)], representing a narrow distribution. A transition in the yield from linear in λ_e^{-1} to quadratic in λ_e^{-1}, as the density of statistically distributed spikes increases, occurs for *all* of the curves presented *if* the calculations are extended sufficiently to large and small Δ_0/λ_e. It is seen that for the range of Δ_0/λ_e relevant to the data, the addition of statistically distributed spikes can represent the trend observed for certain values of $\Delta(0)$ and $\bar{r}$.

The values of the ratios in Fig. 3 show that the energy available based on the linear yields *is* adequate for describing the magnitude of the yields in the quadratic regime for a number of the values of $\Delta(0)$ and $\bar{r}$. That is, no *new* relaxation pathways appear to be needed. However, the behavior in the transition region is very sensitive to $\Delta(0)$ and $\bar{r}$. Because we divide by the linear yields, increasing the initial spike radius, $\Delta(0)$, steepens the transition for a fixed $\bar{r}$. That is, the importance of overlap is larger for spikes with the same $\overline{\Delta E}$ but having a larger initial radius. On the other hand, increasing $\bar{r}$ for a given λ_e and $\Delta(0)$ extends the linear regime by reducing the overlap. (Giving spikes different start times would change $\bar{Y}/Y_l$ similarly.)

Because of the scatter in the data and the possible effect of α_e, we do not attempt to obtain a precise fit to the data by adjusting $\Delta(0)$ and $\bar{r}$. However, for the range of parameters used it is seen that calculations reasonably representative of the data can be obtained in both cases but with different values for the two parameters: Maxwellian, $\Delta(0)\approx\Delta_0$ and $\bar{r}\approx 3\Delta_0$, δ function, $\Delta(0)\approx 9\Delta_0/16$, and $\bar{r}\approx\Delta_0$. The larger values for the Maxwellian distribution are due to the high-energy tail. That is, the Maxwellian distribution is based on local thermodynamic equilibrium; therefore, molecules can have an energy much greater than $\overline{\Delta E}$, albeit with low probability. Since the energy is dispersed by the same collision processes that produce local thermal equilibrium, spikes having a small radius *do not* equilibrate in the early stages when sputtering occurs.[33,34]

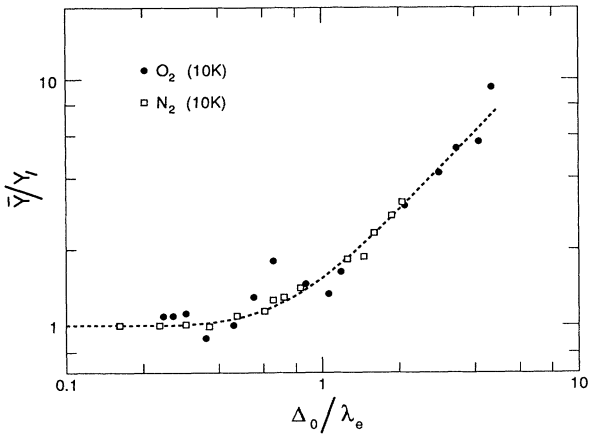

FIG. 2. Data from Tables I and II plotted vs Δ_0/λ_e: for N_2, $\Delta_0\approx 2.1l$ and for O_2, $\Delta_0\approx 2.9l$, where Δ_0 is the intrinsic spike width: $\alpha_e=0.65$ is used to calculate $\lambda_e^{-1}=\alpha_e l(dE/dx_e)/W$.

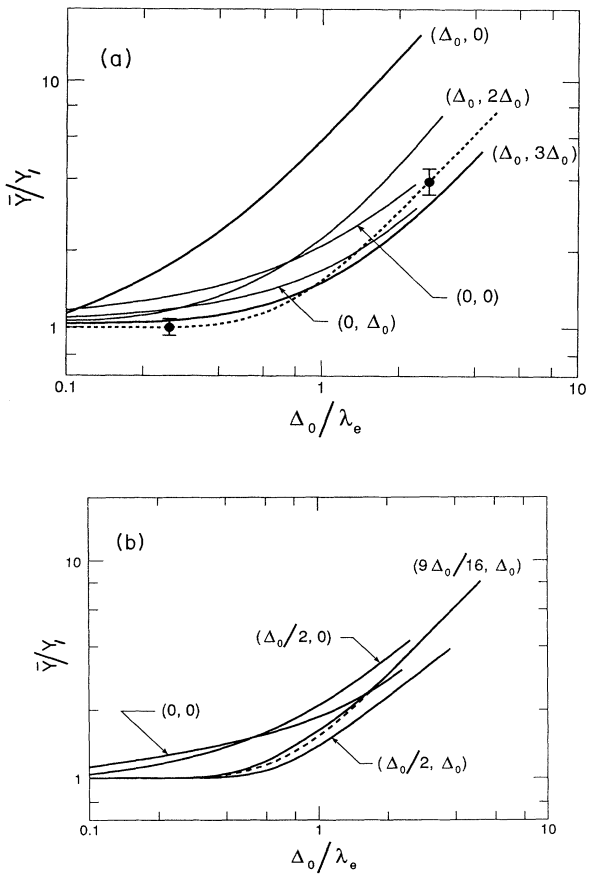

FIG. 3. (a) Solid lines: calculated yield $\bar{Y}$, from the sum of spikes randomly distributed in z for initial widths and radial extent $[\Delta(0),\bar{r}]$ as labeled. Each is divided by the linear yield Y_l obtained in the limit $\lambda_e\to\infty$. Yields are calculated for Maxwellian spikes. Dashed curve: data from Fig. 2. (b) Solid curves: calculated yields divided by linear yield, as in (a), for δ-function spikes distributed in z with initial spike widths and radial extent $[\Delta(0),\bar{r}]$ indicated. Dashed curve: data from Fig. 2.

Although both sets of calculations roughly exhibit the overall trend seen in the data, adjusting $\Delta(0)$ and $\bar{r}$ for the Maxwellian spikes does not give a fit to the data which is nearly as good as the fit obtained for the δ-function distribution in Fig. 3(b) for $\Delta(0)=(9\Delta_0/16)$ and $\bar{r}=\Delta_0$. That is, the sharp bend seen in the data going from linear in λ_e^{-1} to quadratic in λ_e^{-1}, can be reasonably obtained using the δ-function spikes, since the effect of overlap is much less important at the larger λ_e for given values of $\Delta(0)$ and $\bar{r}$. The size of the radial distribution giving a good fit for this case ($\bar{r}\approx\Delta_0\approx 2.1l$ for N_2) is about one third that for the Maxwellian and is consistent with both small distances for excitation transport and with the persistence of linearity, discussed earlier.

VI. CYLINDRICAL SPIKE

To compare to the above we also consider the frequently employed, *ad hoc,* calculation in which the spikes are assumed to evolve individually to give the linear yield, Y_l, ignoring any overlap due to the statistical distribution of spikes. The overlap of the residual energy is then considered by assuming it is distributed uniformly in z forming an energized cylindrical region with some selected initial width. The total yield is taken to be the sum of Y_l [Eq. (4b)] and Y_c [Eq.(3)]. The cylindrical spike yield in Eq. (3), when Φ only depends on the local energy density, can be written[1,3,22,29,39,40] [e.g., Eq. (A8)]

$$Y_c = C\left[\alpha_e f_s l\left[\frac{dE}{dx}\right]_e \Big/ U\right]^2 g(x) \ . \tag{9}$$

Here x is a ratio of the cohesive energy density to the initial energy density in the cylinder

$$x=(n_m U)/(\overline{\Delta E}/2\pi\lambda_e\rho_0^2)=\pi^{-1/2}(2\lambda_e\rho_0^2/\Delta_0^3) \ ,$$

where ρ_0 is the initial cylindrical mean width. As $x\to 0$, $g\to 1$, so the yield is quadratic in λ_e^{-1} at small ρ_0 or small λ_e [Eq. (A10)]. (Johnson[22] evaluates C for a line of spikes truncated at the surface; analytic expressions are given in the Appendix.)

Brown *et al.*[2] used $\rho_0^2=\lambda_e^2+b^2$, where b is the Bohr adiabatic radius for the incident ion (for the He ion speeds, b is about $0.5l$). The yield ratio for this choice of ρ_0 and for $\rho_0=0$ are given in Fig. 4(a) for both Maxwellian and δ-function distributions in the standard model given in the Appendix [Eq. (A9)]. The N_2 data, which have less scatter, are used for comparison since the measured N_2 and O_2 yields are *not* as consistent with each other when displayed as in Fig. 4(a) as they were when the parametrization in Fig. 2 was used. The calculated yields for these ρ_0 are seen *not* to represent the data. Better agreement is obtained by choosing an average ρ_0, independent of λ_e, as in Fig. 4(b). For the Maxwellian distribution the value of $\rho_0\approx 4.1l$ gives a reasonable fit. This is larger than the intrinsic spike radius Δ_0 ($\sim 2.1l$), the Bohr adiabatic radius, and the spike spacings in the transition region ($\sim 3l$). For the yields calculated with the δ-function distribution, $\rho_0\approx 1.6l$, about a third of that for the Maxwellian distribution. In both cases ρ_0 is some average of $\Delta(0)$ and $\bar{r}$ of the previous calculation.

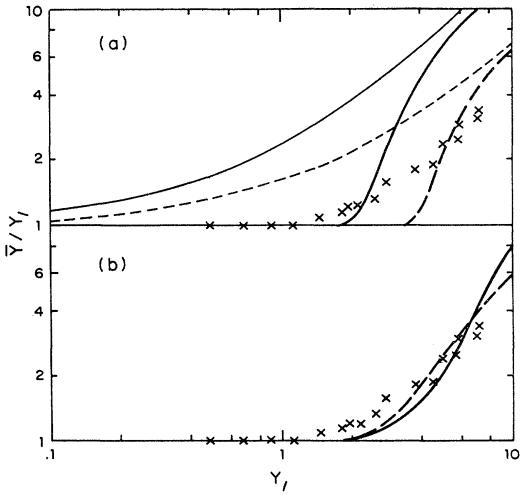

FIG. 4. $\bar{Y}/Y_l$ with $\bar{Y}=Y_l+Y_c$ where Y_l is the linear yield and Y_c is the cylindrical spike yield of Eq. (9). Solid lines are the Maxwellian model, and dashed lines are the δ-function model (see the Appendix). Data shown for N_2 (x). (a) Calculated yields for zero width and darker lines for $\rho_0^2=(\lambda_e^2+b^2)$. (b) Calculated yields for fixed ρ_0 ($4.1l\approx 2\Delta_0$, Maxwellian; $1.6l\approx 3\Delta_0/4$, δ function).

VII. SUMMARY

In this paper we first examined the measured yields for electronic sputtering of N_2 and O_2 and then calculated the transition in the yield from being linear in λ_e^{-1} to being quadratic in λ_e^{-1}. This was done using a statistical distribution of spikes in which each spike is initiated by a repulsive decay event. The driving energy of each spike was assumed to be the same in the linear and quadratic regimes, so that the effect of the overlap of the spikes with decreasing average separation is a more complete use of the released kinetic energy.

The laboratory data indicate that excitation transport is small and that primary ionization alone cannot explain the yields, so that excitations produced by the secondary electrons also contribute to sputtering. The linear regime can be described by minicascades using $\lesssim 12\%$ for N_2 and $\lesssim 37\%$ for O_2 of the total electronic energy deposited in the surface region, corresponding to net average energy depositions $\overline{\Delta E}\lesssim 4.4$ eV and $\lesssim 12$ eV, respectively. The excitation transport (affecting α_e) and the W value in the solid are the most uncertain parameters for determining these energies. Both effects tend to lower the value of $\overline{\Delta E}$. The upper limits are somewhat larger than $\overline{\Delta E}$ given by Brown and co-workers[1,4] and Ellegard and co-workers;[7,9] the earlier values of Rook, Johnson, and Brown[24] are comparable if $\alpha_e\approx 1$. The $\overline{\Delta E}$ for N_2 is roughly consistent with the ejected particle energies measured by Pedrys *et al.*,[25] suggested to involve an average of a number of processes of different energies.

In describing the linear-to-quadratic transition in electronic sputtering, processes that depend on the excitation density could, in principle, be important, as suggested for CO,[43] such as the cooling of secondary electrons,[41] radia-

tive losses, and new nonradiative pathways. Also, lower energy events, ignored in the linear regime e.g., vibrational excitation,[42] could, in principle, participate in the sputtering. However, the agreement with the data for the calculations performed here, in which such changes were ignored, indicate that over the $(dE/dx)_e$ range covered additional energy sources are *not needed* in the quadratic regime. The local energy density at the surface was used to calculate the yield employing a surface flux determined by either a Maxwellian or a "δ-function" distribution of energies in the "minispike" associated with each excitation. For comparison, the *ad hoc* model of adding a linear yield to a "cylindrical spike" yield was also calculated using these two energy distributions. The use of the δ-function distribution in the statistical calculation gave the best agreement with the two data sets. The steepness of the linear-to-quadratic transitions observed in the electronic sputtering yield for N_2 and O_2 requires that the events be radially distributed about the incident ion path. Larger radial distributions are required for the broad than for the narrow spikes due to the unrealistic, high-energy tails in the energy distribution of the former, as reflected in the expression for surface flux Φ. The mean radial distribution ($\sim 1.2l$ for the δ-function spikes) is also consistent with very little excitation transport prior to nonradiative relaxation, unlike what was found for solid Ar (Ref. 6).

The calculations described here show that a model based on randomly distributed spikes that produce sublimation can be used to describe the linear-to-quadratic transitions in the electronic sputtering yield for N_2 and O_2. Earlier it was shown analytically that the dependence of yield in the quadratic regime on angle of incidence[22] could be described by a sum of such spikes. It is also seen here that the measured sputtering yields can be used to place constraints on the conversion of the electronic energy deposited into kinetic energy, the extent of excitation transport, and the description of the energy distribution at the surface.

ACKNOWLEDGMENTS

Work supported by National Science Foundation (NSF) Astronomy Division Grant No. AST-85-11391 and NSF Division of Materials Research Grant No. DMR-86-00469.

APPENDIX

Calculation of $\Delta\bar{z}$

A number of related expressions for $\Delta\bar{z}$ are in the literature.[1,9–11,31–33] For collision cascade sputtering, by a point source

$$\Delta\bar{z}=\delta(3/2\pi^2)(\overline{\Delta E}/U)/(n_m\bar{\sigma}_d)\ , \tag{A1}$$

when $\overline{\Delta E} \gg U$. The factor δ accounts for a depletion in the effect of the cascade due to the presence of the surface, n_m is the number density, and $\bar{\sigma}_d$ is the transport (diffusion) cross section for the material. Sigmund[31] uses $\delta=\frac{1}{2}$ and $\bar{\sigma}_d \simeq 3.6$ Å^2 for monatomic metals. Johnson and Brown[1] used $\delta=1$ for the minicascades associated with repulsive relaxation. For condensed gases the species leaving is, predominantly, whole molecules, therefore in Ref. 1 the molecular number density was used for n_m in Eq. (A1) with $\bar{\sigma}_d \alpha n_m^{-2/3}$ and $\delta=1$, so that $(c/n_m\bar{\sigma}_d)\approx 0.15l$ in Eq. (6), $l \approx n_m^{-1/3}$.

Reference 1 used the earlier Sigmund[31] value of $\bar{\sigma}_d$ for atomic rare-gas solids, whereas molecular dynamic simulations[33,34] for low-energy cascades in Ar gave Eq. (A1) with $\bar{\sigma}_d \approx n_m^{-2/3}$, consistent with recent estimates. As atoms were only ejected from the surface layer, Eq. (A1) can be written in terms of the size of the monolayer, l, and an ejection probability, giving

$$\Delta\bar{z}=P_e l,\quad P_e \approx c'(\overline{\Delta E}-U)/U\ , \tag{A2}$$

With $\bar{\sigma}_d \approx n_m^{-2/3}$, c' is equivalent to c in Eq. (6). In the simulations for Ar (Ref. 33), $c' \approx 0.15$; for N_2 (Garrison, private communication) $c' \simeq 0.1$; and for an amorphous O_2 sample,[34] $c' \approx 0.13$. In the text we use $c' \approx 0.14$. Schou co-workers,[9,11] used Eq. (A1) to describe diatomic molecular ejection by considering atomic ejection.[11] Therefore, they use $\frac{1}{2}$ of Eq. (A1) for the molecular yield (as two atoms need to be ejected per molecule) and assumed $\delta=\frac{1}{2}$ with $\bar{\sigma}_d$ equal to Sigmund's old atomic value. The product Un_m in Eq. (A1) is the same for the molecular values and atomic values, so $(c/n_m\bar{\sigma}_d)\approx 0.14l$ for N_2, giving fortuitous agreement in the overall quantity although the cross sections and δ are different.

Spike models

Spike models begin by solving of the diffusion equation

$$\nabla(\kappa\nabla\bar{E})=\left[\frac{\partial\bar{E}}{\partial t}\right]\ , \tag{A3}$$

where we write $\bar{E}$ as the average kinetic energy of the molecules at a point in a material of constant density. This is often described as a temperature implying thermodynamic equilibrium. In other papers we have considered the quantity $n_m\bar{E}$ instead.[3,5,22,29] To obtain the sputter flux, Φ, one needs to make an assumption about the energy spectra. An Arrhenius activation barrier[44] associated with a Maxwell-Boltzmann kinetic energy distribution is used, as is a δ-function energy distribution, in which each atom has the average local energy, $\bar{E}$. If the flux at the surface only depends on the radial position ρ, and time, t, via the value of $\bar{E}$ at the surface,[3,22,29] the yield for a spherical spike at depth z is calculated as

$$Y(z)=\int d^2\rho \int dt\ \Phi(\bar{E}_s(\mathbf{r},t))\ , \tag{A4a}$$

where $r^2=\rho^2+z^2$ and $\bar{E}_s$ is the average energy from Eq. (A3) evaluated at the surface. For the cylindrical spike in Eq. (3),

$$Y_c=\int d^2\rho \int dt\ \Phi(\bar{E}_s(\rho,t))\ . \tag{A4b}$$

The surface flux for the Maxwellian model is[37–40,44–46]

$$\Phi=\Phi_0 y^p \exp(-y^{-1}) \tag{A5a}$$

with $y=kT_s/U$, $\bar{E}\alpha kT$, and Φ is determined by the vapor pressure, the mass of the molecule, M, and the heat capacity. For sublimation the exponent p from the vapor pressure relation varies slowly with the temperature. Here we use the $p=-1/2$ (Ref. 39), but the results shown are relatively insensitive to this power when taking the ratios of yields. We also use $\bar{E}=C_v kT$ with the dimensionless heat capacity, C_v, equal to $\frac{3}{2}$ (i.e., no equilibration with vibration and rotation). For the δ-function distribution,

$$\Phi=\frac{n_m\bar{v}}{4}[1-(U/\bar{E}_s)] \quad \text{for} \quad \bar{E}_s\geq U \ , \tag{A5b}$$

with $\bar{v}=(2\bar{E}/M^{1/2})$, assuming an isotropic velocity distribution and escape limited by planar binding. (Spherical binding may be more appropriate,[17] but this does not affect the yield ratio.) These Φ are used in the statistical calculation as described in Eqs. (1) and (2) with $\bar{E}_s=\sum_i \bar{E}_s(\mathbf{r}_i)$ (Refs. 3 and 22).

For κ constant in Eq. (A3), this gives the spike in Eq. (8), normalized to $\overline{\Delta E}$ $(=\int n_m \bar{E}(r,t)d^3r)$,

$$\bar{E}_s(\mathbf{r}_i,t)=a_s(\overline{\Delta E}/\pi^{3/2}n_m) \times\exp[-r_i^2/\Delta(t)^2]/\Delta(t)^3 \tag{A6}$$

with $\Delta^2=4\kappa(t+t_0)$ and $r_i^2=[(\boldsymbol{\rho}-\boldsymbol{\rho}_i)^2+z_i^2]$. Here $\boldsymbol{\rho}_i$ and z_i give the locations of the spike, $\Delta(0)=(4\kappa t_0)^{1/2}$ is the initial radius, and a_s is a parameter that depends on the ability of the surface to reflect energy ($a_s=1$ for no reflection and $a_s=2$ for perfect reflection[22]). The parameter Δ_0 $[\Delta_0^3=\overline{\Delta E}/(n_m U\pi^{3/2})]$ used below is that spike radius for which $\bar{E}=U$ at $r_i=0$. For a distribution of spikes [viz., Eq. (1a)] the yield is calculated[22]

$$Y_I[\mathbf{r}_1,\mathbf{r}_2,\ldots]=\int d^2\rho\int dt\ \Phi\left[\sum_i \bar{E}_s(\mathbf{r}_i,t)\right] . \tag{A7}$$

This results in the following limiting forms for the average yield, which we used to test our calculations. Assuming the track of events is perpendicular to the surface and $(\Delta_0/\lambda_e)\to 0$ (i.e., large spacing),

$$\bar{Y}\to Y_l=\frac{\pi\Phi_0}{12\kappa}\left[\frac{a_s}{C_v}\right]^{5/3}\Gamma(\tfrac{5}{3}-p)\Gamma(\tfrac{1}{2})(\tfrac{3}{5})^{3/2}(\Delta_0^5/\lambda_e) \quad \text{(Maxwellian)} ,$$

$$=\frac{3\pi n_m}{182\kappa}\left[6\frac{\pi U}{5M}\right]^{1/2}a_s^{5/3}(\Delta_0^5/\lambda_e) \quad (\delta \text{ function}) . \tag{A8a}$$

For $\rho_i \ll \Delta_0$ (i.e., spikes in a line) and $(\Delta_0/\lambda_e)\to\infty$ (i.e., close spacing, a cylindrical spike), using Refs. 5 and 22

$$\bar{Y}\to\begin{cases}\dfrac{\pi^2\Phi_0}{32\kappa}\Gamma(2-p)(a_s\Delta_0^3/C_v\lambda_e)^2 & \text{(Maxwellian)} ,\\ \dfrac{\pi^2 n_m}{480\kappa}\left[\dfrac{2U}{M}\right]^{1/2}(a_s\Delta_0^3/\lambda_e)^2 & (\delta \text{ function}) .\end{cases} \tag{A8b}$$

In these equations Φ_0 comes from Eq. (A5a) and C_v is dimensionless. Also note that (Δ_0^3/λ_e) is proportional to $f_s(dE/dx)_e$. The results in Eqs. (A8a) and (A8b) are linear and quadratic, respectively, in λ_e^{-1}. The linear region, however, shows a somewhat faster scaling with $\overline{\Delta E}$ than found in the simulations.[33,34] Therefore, we display the ratio of $\bar{Y}$ to Y_l versus Δ_0/λ_e, which is only weakly dependent on the choice of $\overline{\Delta E}$ and a_s/C_v.

For the "standard" model in Sec. VI the "heated" region behaves like a high-temperature gas,[39,45,46] $\kappa=\bar{E}^{-1/2}\kappa_0$ (i.e., κ *not* constant) and the cylinder is infinite giving

$$\bar{E}(\rho,t)=\begin{cases}[\epsilon/\Delta(t)^2][1-\rho^2/3\Delta(t)^2]^2, & \rho<(3)^{1/2}\Delta(t)\\ 0, & \rho>(3)^{1/2}\Delta(t) ,\end{cases}$$

with $\epsilon=\Delta\bar{E}/\pi^{3/2}N$, with $N=\Gamma(4)\sqrt{3}/\Gamma(9/2)$. (Note in Ref. 40, p. 188, $\Gamma(\frac{3}{2}-\delta)$ should read $\Gamma(\frac{3}{2}-\delta^{-1})$, $\delta^{-1}=-3$ here.) For this case $\Delta(t)=[14\kappa_0(t+t_0)\epsilon^{1/2}/3]^{2/7}$. The general form for the cylindrical spike yield [viz., Eqs. (3) and (A4b)], like that in Eq. (9), results in

$$\bar{Y}=c(\sigma/U^2)\left[\frac{dE}{dx}\right]_{\text{eff}}^2 g(x) , \tag{A8}$$

based on $\Phi_0=n_m U/(2\pi MU)^{1/2}$ with $p=\frac{1}{2}$ in Eq. (A5a), $\bar{E}=\frac{3}{2}$ kT and $\kappa=a\bar{v}/n\sigma$. For the fastest power-law interaction the appropriate transport cross section[47] is such that $\sigma\approx\bar{\sigma}_d$, and $a\approx 0.6$. Here $g(x)$ depends on the initial width ρ_0 [i.e., $x=2\pi\lambda_e\rho_0^2/\pi^{3/2}\Delta_0^3$]. Equation (A8) can be written in terms of the square of linear yield of Eq. (7), using $(dE/dx)_{\text{eff}}=\alpha_e f_s(dE/dx)_e$ and $(c/n_m\bar{\sigma}_d)\approx 0.15l$; then the quadratic yield is proportional to the square of the linear yield,

$$\bar{Y}=\beta Y_l^2 g(x) . \tag{A9}$$

Here Y_l is the linear yield $[Y_l=(c/n_m\bar{\sigma}_d U)(dE/dx)_{\text{eff}}]$. For the Maxwellian $C\approx 0.02$ in Eq. (9), $\beta\approx 1$, and for the δ-function distribution $C\approx 0.008$, $\beta\approx 0.4$ if $\bar{\sigma}_d\approx l^2$. The width functions are

$$g(x)=\begin{cases}1-x^3\int_x^\infty dt\, e^{-t}/t^2-\int_0^x dt\, e^{-t}t , \\ \text{(Maxwellian)}\\ 1-9x^2+x^3[8-6\ln(x)], \quad 0<x\leq 1\\ (\delta \text{ function})\end{cases} \tag{A10}$$

For the Maxwellian $g(x)$ is evaluated in Refs. 39 and 46 [in Ref. 45, p. 242, $g(x)$ (there $1-g$) is printed incorrectly].

[1]R. E. Johnson and W. L. Brown, Nucl. Instrum. Methods **198**, 103 (1982); **208/210**, 469 (1983).
[2]I. A. Baranov, Yu. V. Martynenko, S. O. Tsepelevich, and Yu. N. Yavlinskii, Usp. Fiz. Nauk **156**, 477 (1988) [Sov. Phys. Usp. **31**, 1015 (1988)]; W. L. Brown, W. M. Augustyniak, K. J. Marcantonio, E. H. Simmons, J. W. Boring, R. E. Johnson, and C. T. Reimann, Nucl. Instrum. Methods B **1**, 304 (1984).
[3]R. E. Johnson, B. U. R. Sundqvist, A. Hedin, and D. Feynö, Phys. Rev. B **40**, 49 (1989).
[4]W. L. Brown, L. J. Lanzerotti, K. J. Marcantonio, R. E. Johnson, and C. T. Reimann, Nucl. Instrum. Methods B **14**, 392 (1986).
[5]K. Gibbs, W. L. Brown, and R. E. Johnson, Phys. Rev. B **38**, 11 001 (1988).
[6]C. T. Reimannn, R. E. Johnson, and W. L. Brown, Phys. Rev. Lett. **53**, 600 (1984); C. T. Reimann, W. L. Brown, and R. E. Johnson, Phys. Rev. B **37**, 1455 (1988).
[7]O. Ellegard, J. Schou, and H. Sørenson, Nucl. Instrum. Methods B **13**, 567 (1986).
[8]J. Schou, P. Børgensen, O. Ellegard, and H. Sørenson, Phys. Rev. B **34**, 93 (1986).
[9]O. Ellegard, J. Schou, H. Sørenson, and P. Børgensen, Surf. Sci. **167**, 474 (1986).
[10]W. L. Brown and R. E. Johnson, Nucl. Instrum. Methods B **13**, 295 (1986).
[11]J. Schou, Nucl. Instrum. Methods B **27**, 188 (1987).
[12]R. Romer, in *Desorption Induced by Electronic Transitions, (DIET) I,* Chemical Phys. Vol. 24, edited by N. H. Tolk *et al.* (Springer, Berlin, 1983), p. 40; P. D. Townsend, in *Sputtering by Particle Bombardment II,* edited by R. Behrisch (Springer-Verlag, Berlin, 1983), p. 147.
[13]K. Tanimura and N. Itoh, Nucl. Instrum. Methods B **46**, 207 (1990).
[14]M. F. Jarrold, A. J. Illies, and M. T. Bowers, J. Chem. Phys. **81**, 222 (1984).
[15]D. A. Thomspon, J. Appl. Phys. **52**, 982 (1981).
[16]D. V. Stenovinovich, D. A. Thompson, and J. A. Davies, Nucl. Instrum. Methods B **1**, 315 (1984).
[17]J. W. Boring, D. J. O'Shaughnessy, and J. A. Phipps, Nucl. Instrum. Methods B **18**, 613 (1987).
[18]P. Sigmund, App. Phys. Lett. **25**, 169 (1974).
[19]H. E. Rosendaal, R. A. Haring, and J. B. Saunders, Nucl. Instrum. Methods **194**, 579 (1982).
[20]C. T. Reimann, J. W. Boring, R. E. Johnson, J. W. Garrett, and K. R. Farmer, Surf. Sci. **147**, 227 (1984).
[21]R. Pedrys, D. J. Oostra, and A. E. deVries in *Desorption Induced by Electronic Transitions, (DIET), II,* edited by W. Brenig and D. Meazel (Springer, Berlin, 1985), p. 190.
[22]R. E. Johnson, J. Phys. (Paris) Colloq. **50**, C2-251 (1989).
[23]A. Hitachi, T. Takahashi, T. Hamada, E. Shibamura, A. Nakomato, N. Funayama, K. Masuda, and T. Doke, Phys. Rev. B **23**, 4779 (1981).
[24]F. L. Rook, R. E. Johnson, and W. L. Brown, Surf. Sci. **164**, 625 (1985).
[25]R. Pedrys, D. J. Oostra, A. Haring, A. E. deVries, and J. Schou, Radiat. Eff. **109**, 239 (1989).
[26]J. F. Ziegler, *Helium: Stopping Powers and Ranges in all Elemental Matter* (Pergamon, New York, 1977); H. H. Andersen and J. F. Ziegler, *Hydrogen: Stopping Powers and Ranges in All Elemental Matter* (Pergamon, New York, 1977).
[27]M. E. Rudd, Y. K. Kim, D. H. Madison, and J. W. Gallagher, Rev. Mod. Phys. **57**, 965 (1985); M. E. Rudd, T. V. Goffe, A. Itoh, and R. D. Dubois, Phys. Rev. A **32**, 829 (1985); M. E. Rudd, T. V. Goffe, and A. Itoh, *ibid.* **32**, 2128 (1985); M. E. Rudd, A. Itoh, and T. V. Goffe, *ibid.* **32**, 2499 (1985).
[28]J. Schou, Phys. Rev. B **22**, 2141 (1980).
[29]R. E. Johnson, Int. J. Mass Spectrom. Ion Phys. **78**, 357 (1987).
[30]J. W. Boring, R. E. Johnson, and D. O'Shaughnessy, Phys. Rev. B 2689 (1989).
[31]P. Sigmund, in *Sputtering by Particle Bombardment,* edited by E. Behrisch (Springer, Berlin, 1981), Vol. 1; Phys. Rev. **184**, 393 (1969).
[32]R. Kelly, in *Ion Beam Modification of Surfaces,* edited by P. Mazzoldi and G. W. Arnold (Elsevier, Amsterdam, 1987), pp. 57–113.
[33]S. T. Cui, R. E. Johsnon, and P. T. Cummings, Surf. Sci. **207**, 186 (1988); S. T. Cui, P. T. Cummings, and R. E. Johnson, *ibid.* **222**, 491 (1989).
[34]S. Banerjee, M. Liu, and R. E. Johnson, Surf. Sci. (to be published).
[35]W. E. Wilson and H. G. Paretzke, Radiat. Res. **87**, 521 (1981); D. J. Brenner and M. Zaider, *ibid.* **98**, 14 (1984); A. E. S. Green and R. P. Singhal, Geophys. Res. Lett. **6**, 625 (1979).
[36]International Commission on Radiation Units Report No. 31, U.S. Dept. of Commerce (Washington, D.C., 1979) (unpublished).
[37]R. Kelly, Nucl. Instrum. Methods B **13**, 283 (1986).
[38]E. Nieschler, B. Nees, N. Bischoff, H. Fröhlich, W. Tiereth, and H. Voit, Surf. Sci. **145**, 294 (1984); A. Mozumder, Ad. Radiat. Chem. **1**, 1 (1969).
[39]P. Sigmund and C. Claussen, J. Appl. Phys. **52**, 990 (1981).
[40]R. E. Johnson and R. Evatt, Radiat. Eff. **52**, 187 (1980).
[41]R. Ritchie and C. Claussen, Nucl. Instrum. Methods **198**, 133 (1982).
[42]P. Williams and B. U. R. Sundqvist, Phys. Rev. Lett. **58**, 1031 (1987).
[43]D. B. Chrisey, W. L. Brown, and J. W. Boring, Surf. Sci **225**, 130 (1990).
[44]G. H. Vineyard, Radiat. Eff. **29**, 245 (1976).
[45]R. E. Johnson, *Introduction to Atomic and Molecular Collision* (Plenum, New York, 1982), pp. 239–243.
[46]C. Claussen, Ph.D. thesis, Odense Universitat, 1984.
[47]S. Chapman and T. G. Cowling, *The Mathematical Theory of Non-Uniform Gases* (Cambridge University, Cambridge, England, 1970).